Journal of Inorganic and General Chemistry
ZAAC
Zeitschrift für anorganische und allgemeine Chemie
DOI: 10.1002/zaac.202000091
ARTICLE

Preparation and Characterization of Protonated Fumaric Acid

Marie C. Bayer,[a] Christoph Jessen,[a] and Andreas J. Kornath*[a]

Dedicated to Dr. Klaus Römer on the Occasion of his 80th Birthday

Abstract. Fumaric acid was reacted with the binary superacidic systems HF/SbF_5 and HF/AsF_5. The *O,O′*-diprotonated $[C_4H_6O_4]^{2+}([MF_6]^-)_2$ (M = As, Sb) and the *O*-monoprotonated $[C_4H_5O_4]^+[MF_6]^-$ (M = As, Sb) species are formed depending on the stoichiometric ratio of the Lewis acid to fumaric acid. The colorless salts were characterized by low-temperature vibrational spectroscopy. In case of the hexafluoridoantimonates single-crystal X-ray structure analyses were carried out. The $[C_4H_6O_4]^{2+}([SbF_6]^-)_2$ crystallizes in the monoclinic space group *C*2/*c* with four formula units per unit cell and $[C_4H_5O_4]^+[SbF_6]^-$ crystallizes in the triclinic space group $P\bar{1}$ with one formula unit per unit cell. The protonation of fumaric acid does not cause a notable change of the C=C bond length. The experimental data are discussed together with quantum chemical calculations of the cations $[C_4H_6O_4 \cdot 4\ HF]^{2+}$ and $[C_4H_6O_4 \cdot 2\ H_2CO \cdot 2\ HF]^{2+}$.

Introduction

Fumaric acid (*trans*-1,2-ethylenedicarboxylic acid) was isolated by *Braconnot* in 1810 from mushrooms.[1] It is used nowadays as food acidulant E297 (pK_{a1} = 3.02 and pK_{a2} = 4.38).[2,3] The strength of commonly used acids is not sufficient for a protonation of fumaric acid. Therefore, *Larsen* et al. investigated fumaric acid in superacidic media. The authors reported an *O,O′*-diprotonation in the superacidic solution FSO_3H/SbF_5 observed by NMR spectroscopy.[4] Furthermore, a study of *Amat* et al. showed that fumaric acid is *O*-monoprotonated in oleum and concentrated sulfuric acid.[5] However, structural parameters as well as vibrational spectroscopic studies are still unkown.[4,5] This prompted us to isolate and structurally characterize salts containing the $[C_4H_6O_4]^{2+}$ and the $[C_4H_5O_4]^+$ cation.

Results and Discussion

Fumaric acid was reacted with the binary superacidic solutions HF/MF_5 (M = As, Sb). To form the $[C_4H_6O_4]^{2+}$ cation an excess of the Lewis acids (AsF_5 or SbF_5) is required [Equation (1)]. The preparation of the salt containing the *O*-monoprotonated cation was carried out according to Equation (2). It is necessary to ensure that an equimolar amount of the Lewis acids with respect to the starting material is used.

Anhydrous hydrogen fluoride (*a*HF) acts as solvent as well as a reagent. The reactions were carried out at a temperature of –20 °C. After the removal of the excess of *a*HF in a dynamic vacuum at –78 °C, the colorless salts $[C_4H_6O_4]^{2+}([SbF_6]^-)_2$ (**1**), $[C_4H_6O_4]^{2+}([AsF_6]^-)_2$ (**2**), $[C_4H_5O_4]^+[SbF_6]^-$ (**3**), and $[C_4H_5O_4]^+[AsF_6]^-$ (**4**) were obtained, which are stable up to 25 °C. Under these reaction conditions no addition of HF to the carbon double bond occurs.

The corresponding deuterated salts $[C_4H_2D_4O_4]^{2+}([SbF_6]^-)_2$ (**5**) and $[C_4H_2D_4O_4]^{2+}([AsF_6]^-)_2$ (**6**) were prepared by varying the superacidic system from HF/MF_5 to DF/MF_5 (M = As, Sb). Since deuterium fluoride is used in large excess, the hydroxy hydrogens are thoroughly replaced by deuterium, leading to a degree of deuteration of approximately 96 %.

Vibrational Spectra of $[C_4H_6O_4]^{2+}([MF_6]^-)_2$ (M = As, Sb)

The low-temperature vibrational spectra of $[C_4H_6O_4]^{2+}([SbF_6]^-)_2$ (**1**), $[C_4H_6O_4]^{2+}([AsF_6]^-)_2$ (**2**) and fumaric acid are shown in Figure 1. The vibrational spectra of the D-isotopomeric salts $[C_4H_2D_4O_4]^{2+}([SbF_6]^-)_2$ (**5**) and $[C_4H_2D_4O_4]^{2+}([AsF_6]^-)_2$ (**6**) as well as deuterated fumaric acid are illustrated in Figure S1 (Supporting Information). In Table 1 selected experimental vibrational frequencies of (**1**) and (**2**) as well as the calculated frequencies of the cation $[C_4H_6O_4 \cdot 4\ HF]^{2+}$ are summarized. The complete table (Table S1) and a table of the vibrational frequencies of fumaric acid (Table S2) are listed in the Supporting Information. The experimental vibrational frequencies of (**5**) and (**6**) together with the calculated frequencies of the cation $[C_4H_2D_4O_4 \cdot 4\ HF]^{2+}$ are given in Table S3 (Supporting Information). According to quantum chemical calculations, which are discussed later, the cation $[C_4H_6O_4]^{2+}$ displays a C_2 symmetry. 36 fundamental vibrations are expected, of which 19 modes are active in the Raman spectra and 17 modes are active in the IR spectra. The assignment of the vibrational modes was carried out by analyzing the Cartesian displacement vectors of the calculated vibrational modes of $[C_4H_6O_4 \cdot 4\ HF]^{2+}$ and by a comparison with the vibrations of fumaric acid.[6,7]

* Prof. Dr A. J. Kornath
E-Mail: andreas.kornath@cup.uni-muenchen.de
[a] Department Chemie
Ludwig-Maximilians-Universität München
Butenandstr. 5–13(D)
81377 Munich, Germany
Supporting information for this article is available on the WWW under **http://dx.doi.org/10.1002/zaac.202000091** or from the author.

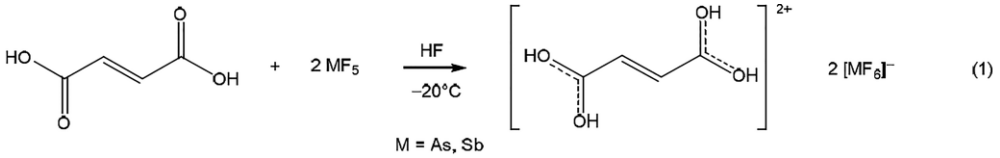

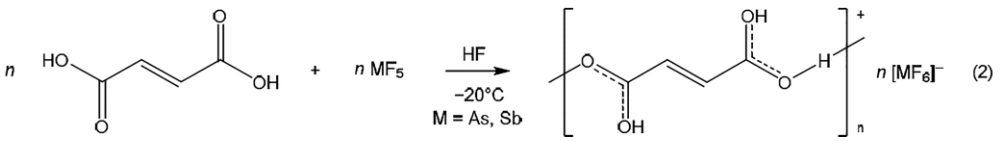

The symmetric C–H stretching mode is detected in the Raman spectra at 3092 cm^{-1} (**1**) and at 3087 cm^{-1} (**2**), respectively. It is blue-shifted by 23 cm^{-1} (**1**) and 18 cm^{-1} (**2**), respectively, compared to that of fumaric acid. Based on the measurement method, moisture condensed on the IR plate. Therefore no meaningful IR bands for the O–H vibrations are observable. In the IR spectra of (**5**) and (**6**) broad bands in the range of 2334 cm^{-1} to 2280 cm^{-1} are observed, as well as in the Raman spectra of (**5**) and (**6**) in the range of 2295 cm^{-1} to 2186 cm^{-1}. In agreement with the theoretical calculations the bands and lines arise from O–D stretching vibrations. The broadening of the IR bands and Raman lines relies on hydrogen bonds in the solid state. The C=C stretching mode occurs at 1686 cm^{-1} (**1**) and at 1684 cm^{-1} (**2**), respectively, and it is blue-shifted by 81 cm^{-1} (**1**) and 79 cm^{-1} (**2**), respectively, compared to fumaric acid. The blue-shift of the C=C stretching mode is due to the positive charge of the ion, resulting from the protonation. The C–O stretching mode is observed at 1637 cm^{-1} (**1**) and 1643 cm^{-1} (**2**), respectively, in the Raman spectra as well as at 1610 cm^{-1} (**1**) and 1612 cm^{-1} (**2**), respectively, in the IR spectra. The C–O stretching vibrations are shifted to lower wavenumbers in comparison to those of the starting material. The shift is a result of the protonation which causes a weakening of the C–O bond.

For the anions $[SbF_6]^-$ and $[AsF_6]^-$ more vibrations are detected than expected for an ideal octahedral symmetry. This indicates a distortion of the octahedral arrangement, which is confirmed by the single-crystal X-ray structural analysis.

Crystal Structure of $[C_4H_6O_4]^{2+}([SbF_6]^-)_2$

The $[C_4H_6O_4]^{2+}([SbF_6]^-)_2$ (**1**) crystallizes in the monoclinic space group *C*2/*c* with four formula units per unit cell. Figure 2 shows the formula unit of (**1**). Selected structural parameters of (**1**) and fumaric acid[8] are listed in Table 2.

The C–O bond lengths are with 1.273(5) Å (C2–O1) and 1.261(5) Å (C2–O2) not significantly different and are in the range between formal C–O single (1.43 Å) and C=O double bonds (1.19 Å).[9] In comparison with fumaric acid,[8] no significant difference of the lengths of the C–OH bonds is observed. The diprotonation causes a significant elongation of the C=O bond lengths of fumaric acid (1.228(4) Å),[8] whereas the C–C and C=C bonds are not significantly affected. The bond angles of fumaric acid are not changed remarkably by

Table 1. Selected experimental vibrational frequencies [cm^{-1}] of $[C_4H_6O_4]^{2+}([MF_6]^-)_2$ (M = As, Sb) and calculated vibrational frequencies [cm^{-1}] of $[C_4H_6O_4 \cdot 4\ HF]^{2+}$.

$[C_4H_6O_4]^{2+}([SbF_6]^-)_2$ (**1**) exp.[a]		$[C_4H_6O_4]^{2+}([AsF_6]^-)_2$ (**2**) exp.[a]		$[C_4H_6O_4 \cdot 4\ HF]^{2+}$ calcd.[b) c)]	Assignment		
IR	Raman	IR	Raman	IR/Raman			
	3092(31)		3087(24)	3040(0/68)	ν_2	A	ν_s(C–H)
	1686(89)		1684(100)	1672(0/185)	ν_4	A	ν(C=C)
	1637(37)		1643(32)	1605(0/126)	ν_5	A	ν(C–O)
1610 m		1612 s		1617(620/0)	ν_{23}	B	ν(C–O)
	1528(13)		1531(12)	1489(0/26)	ν_6	A	ν(C–O)
	1325(11)		1326(19)	1293(0/13)	ν_7	A	δ(CCH)
1279 s		1279 s		1264(229/0)	ν_{25}	B	δ(CCH)
	1281(7)		1272(7)	1264(0/5)	ν_8	A	δ(COH)
1252 m		1250 s		1237(287/0)	ν_{26}	B	δ(COH)
	1233(82)		1223(67)	1220(0/48)	ν_9	A	δ(COH)
1229 s		1217 s		1216(232/0)	ν_{27}	B	δ(COH)
949 s		962 s		950(67/0)	ν_{10}	A	γ(CCH)
	989(24)		985(31)	950(0/8)	ν_{11}	A	ν(C–C)
941 s	952(8)	937 s	956(2)	901(51/0)	ν_{28}	B	ν(C–C)
802 s		797 s		822(256/0)	ν_{13}	A	γ(COH)

a) Abbrevations for IR intensities: vs. = very strong, s = strong, m = medium, w = weak. b) Calculated on the ωB97XD/aug-cc-pVTZ level of theory; scaling factor 0.945. c) IR intensities in km · mol^{-1}; Raman intensities in $Å^4 \cdot u^{-1}$.

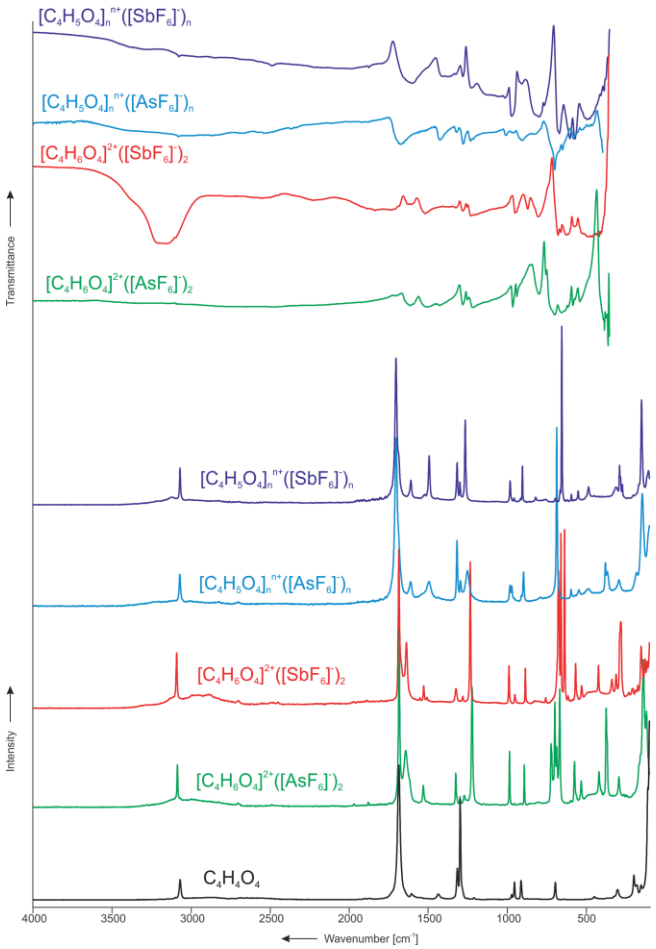

Figure 1. Low-temperature Raman and IR spectra of $[C_4H_6O_4]^{2+}([SbF_6]^-)_2$ (**1**), $[C_4H_6O_4]^{2+}([AsF_6]^-)_2$ (**2**), $[C_4H_5O_4]^+[SbF_6]^-$ (**3**), $[C_4H_5O_4]^+[AsF_6]^-$ (**4**), and the Raman spectrum of $C_4H_4O_4$.

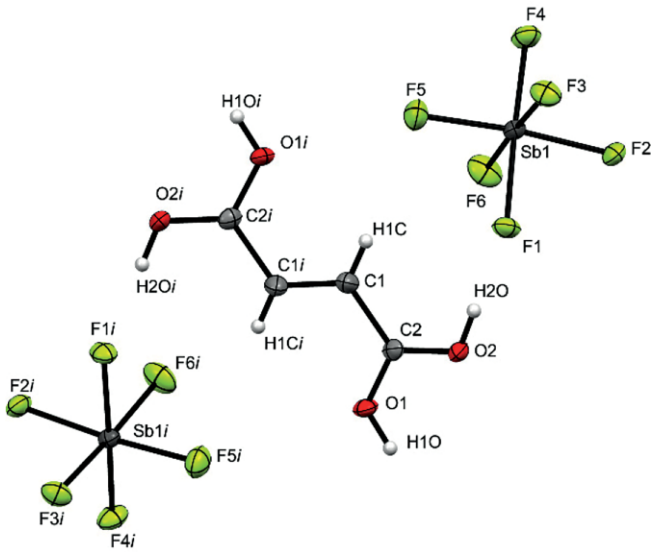

Figure 2. Formula unit of $[C_4H_6O_4]^{2+}([SbF_6]^-)_2$ (displacement ellipsoids with 50 % probability). Symmetry operations: i = 1 –*x*, y, 0.5–z.

the diprotonation. Only the carboxy groups are twisted against one another by 17 ° out of the carbon skeleton plane.

The Sb–F bond lengths in the $[SbF_6]^-$ anion are in the range between 1.913(2) Å and 1.861(2) Å. These values are typical for an $[SbF_6]^-$ anion, indicating a distorted octahedral structure.[10,11] In the crystal packing hydrogen bonds cause an elongation of the Sb1–F1 and Sb1–F2 bonds.

In the solid state of (**1**), the cations and anions are linked by hydrogen bonds with O–H···F donor-acceptor distances in the range of 2.584(4) Å to 2.584(3) Å, which can be categorized as moderate hydrogen bonds in accordance with the classification of *Jeffrey*.[12] The moderate hydrogen bonds O1–H1O···F2*i* and O2-H2O···F1 connect the cations and anions,

Table 2. Selected bond lengths and angles of $C_4H_4O_4$, $[C_4H_6O_4]^{2+}([SbF_6]^-)_2$, and $[C_4H_5O_4]^+[SbF_6]^-$.

	$C_4H_4O_4$ [8]	$[C_4H_6O_4]^{2+}([SbF_6]^-)_2$	$[C_4H_5O_4]^+[SbF_6]^-$
Bond length (Å)			
C1–C1*i* (C=C)	1.315(7)	1.299(9)	1.311(8)
C1–C2 (C–C)	1.490(5)	1.463(6)	1.479(5)
C2–O2 (C=O)	1.228(4)	1.261(5)	1.235(5)
C2–O1 (C–O)	1.289(5)	1.273(5)	1.298(5)
Bond angle [°]			
O1–C2–O2	124.4(7)	120.0(4)	121.3(4)
O1–C2–C1	116.0(6)	117.4(4)	115.3(3)
O2–C2–C1	119.5(6)	122.7(3)	123.5(4)
C1*i*–C1–C2	122.5(8)	121.8(5)	121.7(5)
Angle of torsion [°]			
O1–C2–C1–C1*i*		16.9(6)	7.1(8)
O2–C2–C1–C1*i*		–162.3(4)	–172.8(6)
C2–C1–C1*i*–C2*i*		178.2(4)	180.0
Donor–acceptor distance [Å]			
O1–H1O···F2*i*		2.584(4)	
O2–H2O···F1		2.584(3)	
O2–H3···O2*iii*			2.425(6)
O1-H2···F2			2.628(4)

forming chains along the *c* axis (Figure S2, Supporting Information).

Vibrational spectra of $[C_4H_5O_4]^+[MF_6]^-$ (M = As, Sb)

The low-temperature vibrational spectra of $[C_4H_6O_4]^{2+}([SbF_6]^-)_2$ (**1**), $[C_4H_5O_4]^+[SbF_6]^-$ (**3**), $[C_4H_5O_4]^+[AsF_6]^-$ (**4**) and fumaric acid are shown in Figure 1. Selected experimental vibrational frequencies of (**3**) and (**4**) and the calculated frequencies of the cation $[C_4H_6O_4 \cdot 2\ H_2CO \cdot 2\ HF]^{2+}$ are summarized in Table 3. The complete table (Table S4) as well as a table of the vibrational frequencies of fumaric acid (Table S2) are summarized in the Supporting Information. According to the quantum chemical calculations, C_1 symmetry is predicted for the cation $[C_4H_5O_4]^+$ with 33 fundamental vibrations. In the solid state the cations are connected via hydrogen bonds leading to the formation of chains, which is discussed later, but it should be noted that this leads to a higher symmetry (C_2) of the cation. The assignment of the vibrational frequencies is based on the analysis of the Cartesian displacement vectors of the calculated vibrational modes of $[C_4H_6O_4 \cdot 2H_2CO \cdot 2HF]^{2+}$ (see the theoretical section below) and on the comparison with the spectra of fumaric acid.[6,7]

The C–H stretching modes of the monoprotonated species observed in the Raman (3070 cm^{-1} for (**3**), 3072 cm^{-1} for (**4**)) and in the IR spectra (3078 cm^{-1} for (**3**), 3082 cm^{-1} for (**4**)), are comparable with those of fumaric acid and are not affected by the protonation. The C=C stretching vibrations of the monoprotonated fumaric acid are observed in the Raman spectra (1704 cm^{-1} for (**3**), 1703 cm^{-1} for (**4**)). These ν(C=C) vibrations are shifted to higher wavenumbers in comparison with those of the diprotonated species and of the starting material. The C=O stretching mode is detected in the Raman spectra at 1609 cm^{-1} for (**3**) and 1611 cm^{-1} for (**4**), respectively. It is red-shifted compared to fumaric acid (1685 cm^{-1}) and the diprotonated species (1637 cm^{-1} for (**1**)). Similarly, the C–O stretching mode displays a large red-shift. Both red-shifts are attributed to the formation of O–H···O bonds. The C–C stretching mode occurs in the Raman spectra (982 cm^{-1} for (**3**), (**4**)) at nearly the same position as for the diprotonated species (989 cm^{-1} (**1**)).

For the anions $[SbF_6]^-$ and $[AsF_6]^-$ more vibrations are observed (see Supporting Information) than expected for an ideal octahedral symmetry, leading to the assumption of distorted octahedral structures. This is confirmed by the results of the single-crystal X-ray structural analysis.

Crystal Structure of $[C_4H_5O_4]^+[SbF_6]^-$

$[C_4H_5O_4]^+[SbF_6]^-$ (**3**) crystallizes in the triclinic space group $P\bar{1}$ with one formula unit per unit cell. Selected structural parameters of (**3**) are given in Table 2. The formula unit of (**3**) is depicted in Figure 3.

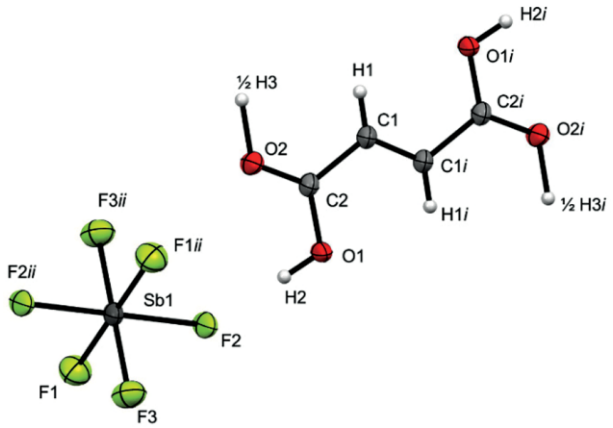

Figure 3. Formula unit of $[C_4H_5O_4]^+[SbF_6]^-$ (displacement ellipsoids with 50 % probability). Symmetry operations: i = –*x*, 2 –*y*, 2 –*z*; ii = 1 –*x*, 1 –*y*, 1 –*z*.

Surprisingly, the carbon-oxygen skeleton of the monoprotonated fumaric acid does not possess significant differences

Table 3. Selected experimental vibrational frequencies [cm^{-1}] of $[C_4H_5O_4]^+[MF_6]^-$ (M = As, Sb) and calculated vibrational frequencies [cm^{-1}] of $[C_4H_6O_4 \cdot 2\ H_2CO \cdot 2\ HF]^{2+}$.

$[C_4H_5O_4]^+[SbF_6]^-$ (**3**) exp.[a]		$[C_4H_5O_4]^+[AsF_6]^-$ (**4**) exp.[a]		$[C_4H_6O_4 \cdot 2H_2CO \cdot 2HF]^{2+}$ calcd.[b) c)]	Assignment		
IR	Raman	IR	Raman	IR/Raman			
3078 w		3082 s		3050(33/0)	ν_{21}	B	ν_{as}(C–H)
	3070(21)		3072(18)	3049(0/80)	ν_2	A	ν_s(C–H)
	1704(82)		1703(94)	1687(0/253)	ν_4	A	ν(C=C)
	1609(14)		1611(14)	1595(0/89)	ν_5	A	ν_s(C=O)
	1494(27)		1495(14)	1491(1/45)	ν_6	A	ν_s(C=O)
	1299(13)		1296(14)	1290(0/25)	ν_8	A	δ(CCH)
1277 m		1275 s		1247(122/0)	ν_{26}	B	δ(CCH)
	1317(24)		1318(37)	1372(1/23)	ν_7	A	δ(COH)
1323 m		1319 m		1365(2776/0)	ν_{25}	B	δ(COH)
	1265(48)		1251(20)	1228(0/47)	ν_9	A	δ(COH)
1225 m		1230 s		1225(779/0)	ν_{27}	B	δ(COH)
1013 s		1007 s		956(40/0)	ν_{11}	A	γ(CCH)
	982(13)		982(12)	946(0/11)	ν_{12}	A	ν(C–C)
905 m		903 s		895(257/0)	ν_{30}	B	ν(C–C)
818 s		822 s		847(222/0)	ν_{13}	A	γ(COH)

a) Abbrevations for IR intensities: vs. = very strong, s = strong, m = medium, w = weak. b) Calculated on the ωB97XD/aug-cc-pVTZ level of theory; scaling factor 0.945. c) IR intensities in km · mol^{-1}; Raman intensities in $Å^4 \cdot u^{-1}$.

to that of fumaric acid (except for the O2–C2–C1 angle). The reasons for this similarity are hydrogen bonds. In the crystal packing of (**3**) the cations are connected via strong hydrogen bonds[12] O–H···O forming chains (Figure 4). The strong hydrogen bond O2–H3···O2*iii* (2.425(6) Å) is formed by two oxygen atoms sharing one proton. Formally only half of a proton is connected to the O2 oxygen atom. Therefore, the formally monoprotonated fumaric acid is better described as a double hemi-protonated fumaric acid. A hemi-protonation has a smaller influence on the C=O bond than a monoprotonation of a carboxy group would have. It should be noted that the crystal packing of fumaric acid itself contains also hydrogen bonds. These hydrogen bonds affect the C=O and C–OH bonds of fumaric acid. Consequently, this leads to the similarity of the carbon-oxygen skeleton of both species.

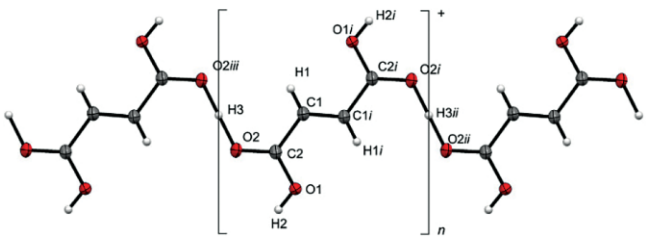

Figure 4. Cation chains in $[C_4H_5O_4]^+[SbF_6]^-$ based on the double hemi-protonation (displacement ellipsoids with 50 % probability). Symmetry operations: i = –*x*, 2 –*y*, 2 –*z*; ii = x, 1+y, z; iii = –*x*, 1 –*y*, 2 –*z*.

In the $[SbF_6]^-$ anion the Sb–F bond lengths are in the range between 1.857(3) Å and 1.895(2) Å, which are in the typical region for $[SbF_6]^-$ anions. Two hydrogen bonds in the crystal packing lead to the Sb1–F2 and Sb1–F2*ii* bond elongation and distortion of the ideal octahedral symmetry.[10,11]

In the solid state, the $[C_4H_5O_4]^+$ chains are linked by the moderate hydrogen bond,[12] O1–H2···F2 (2.628(4) Å) forming layers (Figure S3, Supporting Information).

Quantum Chemical Calculations

The quantum chemical calculations of the free cations $[C_4H_6O_4]^{2+}$ and $[C_4H_5O_4]^+$ were carried out using the B3LYP/aug-cc-pVTZ level of theory. Since hydrogen bonds are involved in the solid state, further calculations were performed. To simulate hydrogen bonds in (**1**) HF molecules were added to the free cation.[16] To simulate the structure of (**3**), one fumaric acid molecule is supplemented by two hydrogen fluoride molecules and two protonated formaldehyde molecules (Figure S4, Supporting Information). The adducts $[C_4H_6O_4 \cdot 4\ HF]^{2+}$ and $[C_4H_6O_4 \cdot 2\ H_2CO \cdot 2\ HF]^{2+}$ were calculated by applying the ωB97XD/ aug-cc-pVTZ level of theory.[17–19] A comparison of the calculated and the experimental cationic structures of $[C_4H_6O_4]^{2+}$ and $[C_4H_5O_4]^+$ is shown in Figure 5. For clarification, the added hydrogen fluoride molecules as well as the formaldehyde molecules are omitted in the case of the calculated structures.

The structural parameters of the adducts are in good agreement with the experimental values (Tables S5 and S6, Supporting Information) and the experimental vibrational frequencies are better represented by the solvated cations (Table S7, Supporting Information).

The C–C and C–O bond lengths of some selected protonated and deprotonated salts containing fumaric acid are summarized in Table 4. Surprisingly, independent of the fumaric acid's charge, no significant difference in the C=C doule bonds is observable. Only the C–C bond length of the dianion is slightly longer than that of the dication. Apart from that, no significant

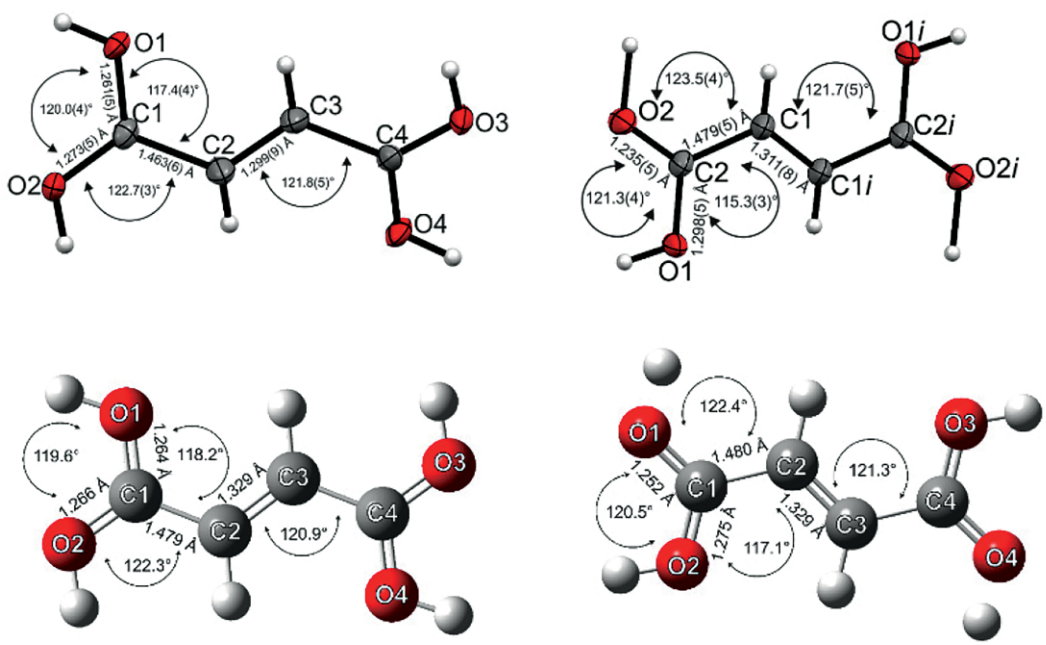

Figure 5. Experimental and calculated cationic structures of $[C_4H_6O_4]^{2+}$ (left) and $[C_4H_5O_4]^+$ (right). The HF molecules as well as the formaldehyde molecules are omitted in the calculated stuctures for clarification.

Table 4. Selected bond lengths of different protonated and deprotonated fumaric acid derivatives.

Chrage of the fumarate backbone	Compound	C=C distance [Å]	C–C distance [Å]	C=O distance [Å]	C–O distance [Å]
–2	$(NH_4)_2C_4H_2O_4$ [14]	1.314(1)	1.496(1)	1.253(1)	1.266(1)
–1	$NaC_4H_3O_4$ [15]	1.327(9)	1.488(8)	1.274(10)	1.287(9)
			1.489(9)	1.227(11)	1.332(8)
0	$C_4H_4O_4$ [8]	1.315(7)	1.490(5)	1.228(4)	1.289(5)
+1	$C_4H_5F_6O_4Sb$	1.311(8)	1.479(5)	1.235(5)	1.298(5)
+2	$C_4H_6F_{12}O_4Sb_2$	1.299(9)	1.463(6)	1.261(5)	1.273(5)

change of the C–C bond lengths is observed. Hydrogen bonds have greater influence on the C–O bonds than the level of protonation or deprotonation. Therefore, varying C–O bond lengths are detected. The carbon-oxygen skeleton of the fumaric acid derivatives remains unchanged regardless of protonation or deprotonation.

Conclusion

Fumaric acid was investigated in the superacidic solutions HF/SbF_5 and HF/AsF_5. The salts of the diprotonated fumaric acid $[C_4H_6O_4]^{2+}([MF_6]^-)_2$ (M = As, Sb) and the monoprotonated fumaric acid $[C_4H_5O_4]^+[MF_6]^-$ (M = As, Sb) were isolated for the first time. The salts were characterized by IR and Raman spectroscopy. Furthermore, single-crystal X-ray structural analyses of $[C_4H_6O_4]^{2+}([SbF_6]^-)_2$ and $[C_4H_5O_4]^+[SbF_6]^-$ are reported. Quantum chemical calculations at the B3LYP/aug-cc-pVTZ and ωB97XD/aug-cc-pVTZ level of theory were considered for the assignment of the vibrational spectra. The C-O and C–C bond lengths do not differ significantly from dianion to dication of fumaric acid. The carbon-oxygen skeleton remains unchanged regardless of protonation or deprotonation.

Experimental Section

Caution! Any contact with the components must be avoided. The hydrolysis of AsF_5, SbF_5, and the reported salts might release HF, burning skin and causing irreparable damage. Adequate safety precautions must be undertaken when handling these materials.

Apparatus and Materials: All experiments were conducted on an electropolished stainless-steel vacuum line. For the syntheses, transparent FEP-reactors with PFA-adapters were employed. To dry the stainless-steel vacuum line and the reaction vessels fluorine was used. Excess fluorine was removed in dynamic vacuum and absorbed by Sodalime. Antimony pentafluoride was handled in a Duran glass high vacuum line using Young valves. Low-temperature Raman spectroscopic measurements were executed on a Bruker® MultiRAMII FT-Raman spectrometer equipped with a Nd:YAG laser (λ = 1064 nm). The interpretation of the spectra was carried out with the aid of the software Advanced Chemistry Development, Inc.® (ACD/Labs 2015). Low-temperature IR spectra were recorded on a Bruker® Vertex-80V-FT-IR spectrometer. The spectra were evaluated using the same software as for the Raman spectra. The low-temperature single-crystal X-ray diffraction was performed on an Oxford XCalibur3 diffractometer equipped with a Spellman generator (50 kV, 40 mA) and a Kappa CCD-detector, operating with $Mo_{K\alpha}$ radiation (λ = 0.7107 Å) at 120 K. Data collection was performed using the CrysAlisCCD software[20] and for the reduction of the data set CrysAlisRED[21] was utilized. For the solution and refinement of the structure the programs SHELXS-97[22] and SHELXL-97[23] integrated in the WinGX software package[24] were employed. The structures were checked with the help of the software PLATON.[25] The absorption correction was carried out using the SCALE3 ABSPACK multiscan method.[26] Crystal data and structure refinement for the reported single-crystal structures are given in Table S8 (Supporting Information). Quantum chemical calculations were carried out using the software package Gaussian09.[27] The theoretical calculations of the naked cations were performed at the B3LYP/aug-cc-pVTZ level of theory. Considering the hydrogen bonds in the solid state, the theoretical calculations of the solvated cations were carried out on the ωB97XD/aug-cc-pVTZ level of theory.

Syntheses of $[C_4H_2X_4O_4]^{2+}([MF_6]^-)_2$ (X = H, D; M = As, Sb): Initially, the Lewis acid AsF_5 or SbF_5 (1.5 mmol) was condensed in a FEP reactor vessel at –196 °C together with anhydrous hydrogen fluoride (*a*HF) or deuterium fluoride (*a*DF) (2 mL). To form the superacidic system, both components were warmed up in static vacuum to –20 °C and homogenized. At –196 °C the superacidic mixture was refrozen. Afterwards, fumaric acid (0.5 mmol) was added to the frozen mixture under nitrogen atmosphere. The reaction mixture was warmed in static vacuum up to –20 °C at which the reaction occurs. In dynamic vacuum excess solvent was removed within 14 h at –78 °C. Colorless crystalline solids were formed in all of these experiments.

Syntheses of $[C_4H_2X_3O_4]^+[MF_6]^-$ (X = H, D; M = As, Sb): The Lewis acid AsF_5 or SbF_5 (1.0 mmol) was condensed in a FEP reactor vessel followed by *a*HF or *a*DF (2 mL) at –196 °C. The mixture was warmed up to –20 °C and mixed to ensure the formation of the superacid. Accordingly, the mixture was refrozen at –196 °C. $C_4H_4O_4$ (1.0 mmol) was added to the frozen mixture under inert gas atmosphere. The reaction mixture was then warmed up to –20 °C and mixed until a colorless solution was received. Excess solvent was removed at –78 °C in dynamic vacuum. Colorless crystalline solids were obtained in all of the experiments.

Supporting Information (see footnote on the first page of this article): The supporting information contains the low-temperature IR and Raman spectra of $[C_4H_2D_4O_4]^{2+}([SbF_6]^-)_2$ (**5**), $[C_4H_2D_4O_4]^{2+}([AsF_6]^-)_2$ (**6**) and deuterated fumaric acid (Figure S1); Experimental vibrational frequencies [cm^{-1}] of $[C_4H_6O_4]^{2+}([MF_6]^-)_2$ (M = As, Sb) and calculated vibrational frequencies [cm^{-1}] of $[C_4H_6O_4 \cdot 4\ HF]^{2+}$ (Table S1); Experimental vibrational frequencies [cm^{-1}] of fumaric acid in comparison with literature data[6,7] (Table S2); Experimental vibrational frequencies [cm^{-1}] of $[C_4H_2D_4O_4]^{2+}([MF_6]^-)_2$ (M = As, Sb) and calculated vibrational frequencies [cm^{-1}] of $[C_4H_2D_4O_4 \cdot 4\ HF]^{2+}$ (Table S3); Detail of the crystal structure of $[C_4H_6O_4]^{2+}([SbF_6]^-)_2$. (Displacement ellipsoids with 50% probability) (Figure S2); Experimental vibrational frequencies [cm^{-1}] of $[C_4H_5O_4]^+[MF_6]^-$ (M = As, Sb) and calculated vibrational frequencies [cm^{-1}] of $[C_4H_6O_4 \cdot 2\ H_2CO \cdot 2\ HF]^{2+}$ (Table S4); Layers formed by hygrogen bonds in $[C_4H_5O_4]^+[SbF_6]^-$. (Displacement ellipsoids with 50% prob-

ability) (Figure S3); Quantum chemical calculated structure of simulated double hemi-protonated fumaric acid under consideration of hydrogen bonds in the solid state $[C_4H_6O_4 \cdot 2\ H_2CO \cdot 2\ HF]^{2+}$ (Figure S4); Selected experimental obtained and calculated bond lengths and angles of the $[C_4H_6O_4]^{2+}$ cation. Symmetry operations: i = C_2-Rotation (Table S5); Selected experimentally obtained and calculated bond lengths and bond angles of the naked and the solvated cation $[C_4H_5O_4]^+$. Symmetry operations: i = C_2-Rotation (Table S6); Selected experimental vibrational frequencies [cm^{-1}] of $[C_4H_5O_4]^+[MF_6]^-$ (M = As, Sb) and calculated vibrational frequencies [cm^{-1}] of $[C_4H_5O_4]^+$ and $[C_4H_6O_4 \cdot 2\ H_2CO \cdot 2\ HF]^{2+}$ (Table S7); and crystal data and structure refinement of $[C_4H_6O_4]^{2+}([SbF_6]^-)_2$ and $[C_4H_5O_4]^+[SbF_6]^-$ (Table S8).

Acknowledgements

We gratefully acknowledge the financial support of the Deutsche Forschungsgemeinschaft (DFG), the Ludwig-Maximilians-Universität (LMU), and the F-Select GmbH.

Keywords: Fumaric acid; Quantum chemical calculations; Superacidic systems, Vibrational spectroscopy; X-ray structure analyses

References

[1] W. Karrer, *Konstitution und Vorkommen der organischen Pflanzenstoffe*. *Exclusive Alkaloide*, Birkhäuser Basel, Basel, s. l., **1958**.
[2] H.-D. Belitz, W. Grosch, P. Schieberle, *Lehrbuch der Lebensmittelchemie*. *Mit 634 Tabellen*, Springer, Berlin, Heidelberg, **2008**.
[3] David R. Lide, CRC Handbook of Chemistry and Physics, Internet version, CRC Press, Boca Raton, FL, **2005**.
[4] J. W. Larsen, P. A. Bouis, *J. Org. Chem.* **1973**, *38*, 1415.
[5] A. M. Amat, G. Asensio, M. J. Castello, M. A. Miranda, A. Simon-Fuentes, *Tetrahedron* **1987**, *43*, 905.
[6] https://sdbs·db.aist.go.jp (National Institute of Advanced Industrial Science and Technology, 21.05.2019).
[7] Y. Du, H. X. Fang, Q. Zhang, H. L. Zhang, Z. Hong, *Spectrochim. Acta Part A Mol. Biomolecular. Spectrosc.* **2016**, *153*, 580.
[8] A. L. Bednowitz, B. Post, *Acta Crystallogr.* **1966**, *21*, 566.
[9] E. Wiberg, N. Wiberg, A. F. Holleman, *Anorganische Chemie*, 103. Aufl., De Gruyter, Berlin, Boston, **2017**.
[10] R. Minkwitz, C. Hirsch, T. Berends, *Eur. J. Inorg. Chem.* **1999**, *1999*, 2249.
[11] R. Minkwitz, S. Schneider, *Angew. Chem.***1999**, *111*, 229.
[12] G. A. Jeffrey, *An Introduction to Hydrogen Bonding*, *Topics in Physical Chemistry*, Oxford University Press, New York, **1997**.
[13] M. P. Gupta, B. N. Sahu, *Acta Crystallogr., Sect. B Struct. Crystallogr. Cryst. Chem.* **1970**, *26*, 1969.
[14] H. Hosomi, Y. Ito, S. Ohba, *Acta Crystallogr., Sect. C Cryst. Struct. Commun.* **1998**, *54*, 142.
[15] M. P. Gupta, R. G. Sahu, *Acta Crystallogr., Sect. B Struct. Crystallogr. Cryst. Chem.* **1970**, *26*, 1964.
[16] T. Soltner, N. R. Goetz, A. Kornath, *Eur. J. Inorg. Chem.* **2011**, *2011*, 3076.
[17] K. S. Thanthiriwatte, E. G. Hohenstein, L. A. Burns, C. D. Sherrill, *J. Chem. Theory Computation* **2011**, *7*, 88.
[18] M. D. Struble, C. Kelly, M. A. Siegler, T. Lectka, *Angew. Chem. Int. Ed.* **2014**, *53*, 8924.
[19] L. A. Burns, A. Vázquez-Mayagoitia, B. G. Sumpter, C. D. Sherrill, *J. Chem. Phys.* **2011**, *134*, 84107.
[20] CrysAlisCCD, Version 1.171.35.11 (release 16–05–2011 CrysAlis 171.NET), Oxford Diffraction Ltd, UK, **2011**.
[21] CrysAlisRED, Version 1.171.35.11 (release 16–05–2011 CrysAlis 171.NET), Oxford Diffraction Ltd, UK, **2011**.
[22] G. M. Sheldrick, *SHELXS-97*, Program for Crystal Structure Solution, University of Göttingen, Germany, **1997**.
[23] G. M. Sheldrick, *SHELXL-97*, Program for Crystal Structure Solution, University of Göttingen, Germany, **1997**.
[24] L. J. Farrugia, *J. Appl. Crystallogr.* **1999**, *32*, 837.
[25] A. L. Speck, *PLATON*, A Multipurpose Crystallographic Tool, Utrecht University, Utrecht, Netherlands, **1999**.
[26] SCALE3 ABSPACK, An Oxford Diffraction Program, Oxford Diffraction Ltd, UK, **2005**.
[27] M. J. Frisch, G. W. Trucks, H. B. Schlegel, G. E. Scuseria, M. A. Robb, J. R. Cheeseman, G. Scalmani, V. Barone, B. Mennucci, G. A. Petersson, H. Nakatsuji, M. Caricato, X. Li, H. P. Hratchian, A. F. Izmaylov, J. Bloino, G. Zheng, J. L. Sonnenberg, M. Hada, M. Ehara, K. Toyota, R. Fukuda, J. Hasegawa, M. Ishida, T. Nakajima, Y. Honda, O. Kitao, H. Nakai, T. Vreven, J. A. Montgomery, J. E. Peralta, F. Ogliaro, M. Bearpark, J. J. Heyd, E. Brothers, K. N. Kudin, V. N. Staroverov, R. Kobayashi, J. Normand, K. Raghavachari, A. Rendell, J. C. Burant, S. S. Iyengar, J. Tomasi, M. Cossi, N. Rega, J. M. Millam, M. Klene, J. E. Knox, J. B. Cross, V. Bakken, C. Adamo, J. Jaramillo, R. Gomperts, R. E. Stratmann, O. Yazyev, A. J. Austin, R. Cammi, C. Pomelli, J. W. Ochterski, R. L. Martin, K. Morokuma, V. G. Zakrzewski, G. A. Voth, P. Salvador, J. J. Dannenberg, S. Dapprich, A. D. Daniels, O. Farkas, J. B. Foresman, J. V. Ortiz, J. Cioslowski, D. J. Fox, *Gaussian09, Revision A.02*, Gaussian, Inc, Wallingford CT, **2009**.

Received: February 24, 2020

